ISBN: 978-3-95450-214-1 ISSN: 2673-5490 doi:10.18429/JACoW-IPAC2021-THXB01

3D TRACKING OF A SINGLE ELECTRON IN IOTA *

A. Romanov†, S. Nagaitsev, J. Santucci, G. Stancari, A. Valishev
Fermi National Accelerator Laboratory, Batavia, IL , USA
N. Kuklev, I. Lobach, The University of Chicago, Department of Physics, Chicago, IL, USA

Abstract

High-resolution observations of single-particle dynamics have the potential as a powerful tool in the diagnostics, tuning and design of storage rings. We are presenting the results of experiments with single electrons that were conducted at Fermilab's IOTA ring to explore the feasibility of this approach. A set of sensitive, high-resolution digital cameras was used to detect the synchrotron radiation emitted by an electron, and the resulting images were used to reconstruct the time evolution of oscillation amplitudes in all three degrees of freedom. From the evolution of the oscillation amplitudes, we deduce transverse emittances, momentum spread, damping times, beam energy and estimated residual-gas density and composition. To our knowledge, this is the first time that the dynamics of a single particle in a storage ring has been tracked in all three dimensions. We discuss further development of a single-particle diagnostics that may allow reconstruction of its turn-by-turn coordinates over macroscopic periods of time facilitating ultra-precise lattice diagnostics and direct benchmarking of tracking codes.

INTRODUCTION

Observation of a single electron in storage rings has a long history that goes back to experiments at AdA, the first electron-positron collider [1, 2]. Observation of discrete steps in radiation intensity offers unique metrology capabilities associated with the absolute calibration of circulating currents and radiation properties [3–5]. Another set of experiments was focused on measurements of synchrotron oscillations by registering deviations of photon arrival times with respect to the revolution reference signal [6–8]. A decade ago, advancements in digital imaging technology allowed experimenters to obtain digital images of radiation from single circulating electrons, but exposure times were too long to resolve and track instantaneous oscillation amplitudes [9].

This paper presents the results of a first series of experiments dedicated to a systematic study of an electron's dynamics in the longitudinal and transverse planes by analyzing high-resolution digital images obtained with sensitive cameras [10]. The experiments were carried out in March 2019 during IOTA Run 1. Studies on the precise measurement of photon arrival times will be presented separately.

* This work was supported by the U.S. National Science Foundation under award PHY-1549132, the Center for Bright Beams. Fermi Research Alliance, LLC operates Fermilab under Contract DE-AC02-07CH11359 with the US Department of Energy.
† aromanov@fnal.gov

THE IOTA STORAGE RING

The Integrable Optics Test Accelerator (IOTA) was recently commissioned with 100 MeV/*c* electrons as part of the Fermilab Accelerator Science and Technology (FAST) facility [11, 12]. IOTA is a storage ring with a circumference of 40 m (Fig. 1). It can store electron or proton beams at momenta between 50 and 150 MeV/*c* and it can be reconfigured to accommodate different experiments. The main goal of IOTA is to demonstrate the advantages of nonlinear integrable lattices for high-intensity beams and to demonstrate new beam cooling methods [11, 13]. Low-emittance and highly configurable electron bunches are injected from the FAST superconducting linac [14, 15].

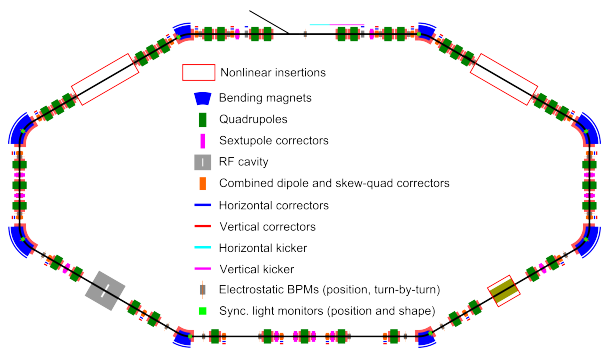

Figure 1: IOTA schematic layout.

Precise beam position and shape measurements are necessary to tune IOTA lattice parameters to the required level [16]. Therefore during IOTA design and construction, special attention was given to beam diagnostics. The main set consists of the following components: wall-current monitor; direct-current current transformers; 21 electrostatic pickups (BPMs); 2 synchrotron-radiation photomultipliers (PMTs) and 8 synchrotron-radiation cameras.

During the experiments presented in this paper, IOTA operated with 100 MeV electrons and was configured for experiments with one special nonlinear insertion, either a string of nonlinear Danilov-Nagaitsev magnets [13, 17] or an octupole channel to generate a Hénon-Heiles potential [18, 19]. Table 1 lists the beam parameters at the time of the experiments.

Synchrotron-Light Detection

Each of the 8 main dipoles in IOTA is equipped with synchrotron light stations installed on top of the magnets themselves. The light out of the dipoles is deflected upwards and back to the horizontal plane with two 90-degree mirrors. A focusing lens and an iris are installed between the two mirrors. After the second mirror, the light enters the dark

ISBN: 978-3-95450-214-1 ISSN: 2673-5490 doi:10.18429/JACoW-IPAC2021-THXB01

Table 1: IOTA Electron Beam Parameters

Parameter	Value
Perimeter	39.96 m
Momentum	100 MeV/c
Electron current	0–4.8 mA
RF frequency	30 MHz
RF voltage	250 V
Betatron tunes, (ν_x, ν_y)	(0.28, 0.31)
Synchrotron tune, ν_s	$3.5 \cdot 10^{-4}$
Damping times, (τ_x, τ_y, τ_s)	(6.15, 2.38, 0.91) s
Horizontal emittance, ϵ_x	36.6 nm
Momentum spread, $\Delta p/p$	$8.4 \cdot 10^{-5}$
Momentum compaction	0.077

box, which is instrumented with customizable diagnostics, as shown in Fig. 2. At the time of the experiment, 7 magnets were equipped with sensitive digital cameras. Cameras BFLY-PGE-23S6M-C from the Point Grey company (now FLIR) were used during the presented studies, they have around 80% quantum efficiency in the visible spectrum and low dark and readout noise. It turns out that the sensitivity of the cameras is high enough to provide images even for a single electron circulating in the ring for relatively short exposure times (fractions of a second).

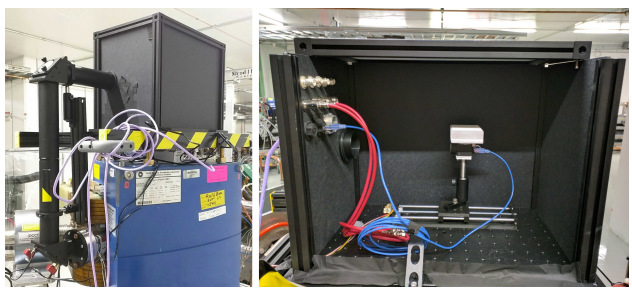

Figure 2: General view of a synchrotron-radiation station at a 60-degree dipole (left). The interior of the dark box (right), with a passively cooled camera.

A single 100 MeV electron circulating in the IOTA ring produces about 7,500 detectable photons per second [20], as confirmed by measurements with the photomultipliers. This intensity is enough to be easily detected by a PMT or by a digital camera. In IOTA, both PMTs [21] and cameras are routinely used to study beams with intensities from a single electron up to the maximum current. About 10 photons per pixel are necessary to exceed the background noise level on a camera. This puts a limit on the size of the light spot at the camera sensor.

AMPLITUDE RECONSTRUCTION METHOD

The oscillation amplitudes of the electron trajectories were obtained by comparing synchronized sets of images with a model describing the expected projections of these images onto the horizontal and vertical axes.

The scaling factors and rolls for each camera were measured basing on closed-orbit responses of both cameras and electrostatic pickups to dipole trims and RF frequency modulation, using the LOCO technique [22–24].

In the absence of linear coupling, the image of a single electron at a position with beta functions β_x and β_y and dispersion D_x is the time average over the revolutions n of the corresponding oscillations with mode-amplitudes A_x, A_y, and A_p:

$$\begin{aligned} x &= A_x\sqrt{\beta_x}\cos(\psi_{x,n}) + A_{\Delta p/p}D_x\cos(\psi_{p,n}), \\ y &= A_y\sqrt{\beta_y}\cos(\psi_{y,n}). \end{aligned} \tag{1}$$

In order to avoid confusion between mode-amplitudes and oscillation amplitudes corresponding to a specific beta-function or dispersion, latter will be denoted by capital letters of the corresponding planes:

$$X_\beta = A_x\sqrt{\beta_x}, \quad Y_\beta = A_y\sqrt{\beta_y}, \quad X_p = A_{\Delta p/p}D_x. \tag{2}$$

The 1-dimensional probability density for a particle that executes a single-mode oscillations with amplitude R is:

$$\rho_1(R,r) = \begin{cases} \frac{1}{\pi\sqrt{R^2-r^2}} & \text{for } |r| \le R, \\ 0 & \text{for } |r| > R. \end{cases} \tag{3}$$

A projection of two-mode oscillation, like in horizontal plane is a result of convolution of two corresponding single-mode projections. To account for finite resolution of the images another convolution with a point spread function (PSF) was made. Because of a limited resolution all blurring effects were accounted with a single PSF of a truncated Gaussian with a cutoff at 2 standard deviations.

Figure 3 shows model projections for single- and two-mode oscillations with and without convolution with PSF. The projection of two independent oscillations has a distinct shape, with peaks at $\pm(R_1 - R_2)$ and shoulders that extend to $\pm(R_1 + R_2)$ in the case of a narrow PSF, where R_1 and R_2 are two mode amplitudes. Having a feature of the image projections that depends linearly on a small amplitude makes it easier to resolve both amplitudes, especially in comparison with the case of a beam profile with a nearly Gaussian shape. In the latter case, the smooth profile depends on the small amplitude only quadratically making it harder to resolve.

EXPERIMENTAL RESULTS

Single Electron Injection

Several steps were taken to inject a small number of electrons in IOTA. First, the laser of the FAST linac photoinjector was switched off, so that only dark current was generated. Three OTR foils were inserted along the injector to further reduce intensity. Fine control of the attenuation was achieved by using the last quadrupole before the IOTA

ISBN: 978-3-95450-214-1 ISSN: 2673-5490 doi:10.18429/JACoW-IPAC2021-THXB01

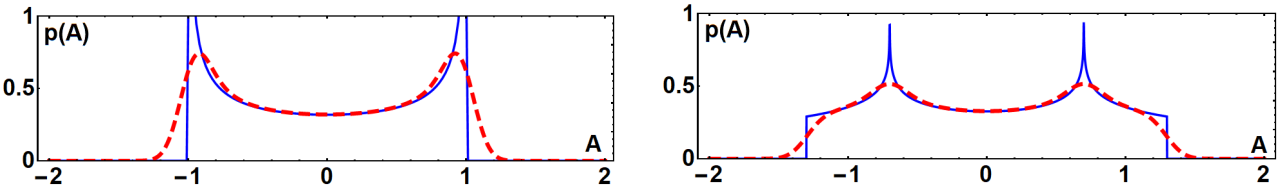

(a) One oscillation mode (b) Two oscillation modes

Figure 3: Model projections for the cases of one and two modes, with and without smearing due to a Gaussian PSF (dashed red lines and solid blue lines, respectively). The amplitude of the first mode is 1 (arb. units), the second amplitude is 0.3, and the standard deviation of the PSF is 0.1.

injection kicker. As a result, it was possible to obtain a distribution for the number of injected particles with peak and average near 1 electron and probability of such injection of about 30%. If needed, it was also possible to remove electrons from the circulating beam, one at a time, by carefully lowering the voltage of the IOTA RF cavity and then quickly restoring it to the nominal value.

Lifetime of a Beam with Countable Number of Electrons

The lifetime of a beam with about one hundred electrons was measured during the same shift as the single-electron studies. The camera settings were the same. The maximum number of electrons in the ring for this data set was chosen to avoid saturation of the core pixels.

Figure 4 shows the total signal from all cameras in an elliptical region of interest (10 and 12.5 beam standard deviations in horizontal and vertical, respectively), normalized to the size of the discrete steps due to single-electron losses. First 1000 seconds are shown.

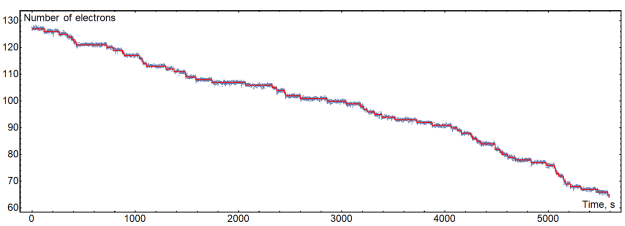

Figure 4: Number of circulating electrons in IOTA as a function of time. Beam intensity measured as the sum of pixel signals in the regions of interest of all 7 cameras, normalized to the single-electron step size. The red line is a best fit to the data with integer numbers of electrons.

Estimation of the lifetime was made basing on analysis of a discrete steps of integral intensity from all cameras following method described in [25]. For this data set, the beam lifetime was 9100(1200) s or 2.52(32) h.

Evolution of Single Electron Oscillation Amplitudes

The analysis presented here is based on a series of 2876 sets of images. Each set consists of synchronized images from 7 cameras with exposures of 0.5 s and delays of 0.2 s between them. The delay was necessary to read out and save raw frames to a hard drive. A median filter with a 2 pixel radius and a moving average filter with a radius of 5 pixels were applied to each image to reduce noise.

For robust estimates of the uncertainties on the model parameters, we used the bootstrap method. The method is also useful to detect anomalies in the fitting process. For each set of synchronized image projections, 25 synthetic bootstrap samples were generated and the corresponding distribution of fit parameters was calculated.

Figure 5 shows an image from the M2L camera, together with its horizontal and vertical measured and fitted projections. A synchronized groups of 7 images were used to reconstruct each set of 3 mode amplitudes. Figure 6 shows the fitted amplitudes and their statistical uncertainties during the first 150 seconds of observations. The 3 planes exhibit different patterns, in general. The horizontal plane has a damping time that is large compared to the camera exposure time. Amplitudes are large enough to be reliably resolved. Random fluctuations, mostly driven by fluctuations of synchrotron radiation emission, can be seen. Synchrotron oscillations have the shortest damping time, which is comparable to the exposure duration. Therefore, the reconstructed amplitude is close to the equilibrium value. In the vertical plane, amplitude excitations from synchrotron radiation are very small — what is observed are relatively sparse interactions with the residual gas.

Figure 7 shows histogram of betatron amplitudes in the horizontal plane. It has good agreement with a distribution of amplitudes in a Gaussian beam.

Autocorrelation functions of the squared mode amplitudes were used to extract damping times τ. In case of a Normal beam distribution it can be described by following formula:

$$\langle A(t)^2 A(t+\Delta t)^2 \rangle_{t,\Delta t} = 4A_0^4 \left(1 + \exp^{-2\Delta t/\tau}\right). \quad (4)$$

Figure 8 shows plot of the autocorrelation function calculated for betatron amplitudes in the horizontal plane.

Figure 9 shows a histogram of the measured vertical amplitude distribution, normalized to a location with $\beta_y = 1$ m. The finite resolution of the optical systems allowed us to reliably resolve amplitudes above 30 m (relative to the same $\beta_y = 1$ m). The tail of the distribution formed by scattering on a residual gas atoms doesn't follow exponential decay. We found following empirical distribution that fits ampli-

ISBN: 978-3-95450-214-1 ISSN: 2673-5490 doi:10.18429/JACoW-IPAC2021-THXB01

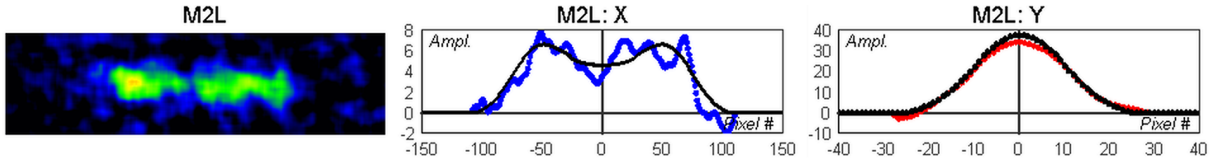

Figure 5: A sample image from the M2L camera, together with their horizontal (center) and vertical (right) projections. The blue and red curves show the experimental data, whereas the black curves represent the fitted model projections.

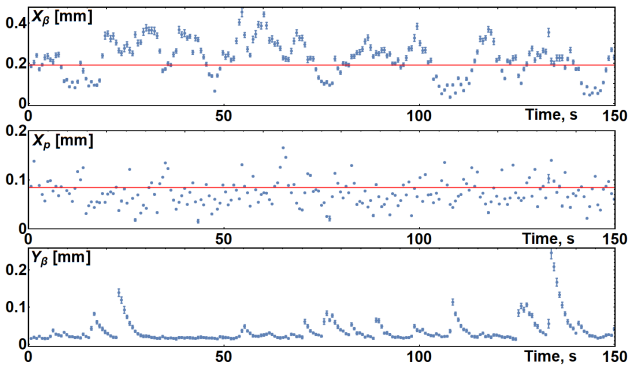

Figure 6: Measured amplitudes for betatron oscillations in horizontal (top), and vertical (bottom) planes at a location with 1 m beta functions, and for horizontal amplitude from synchrotron oscillations (middle) for a diapersion of 1 m. The red lines show the calculated equilibrium amplitudes.

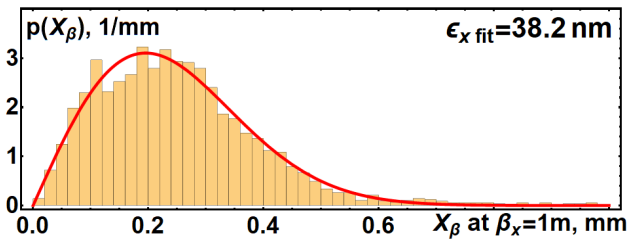

Figure 7: Histogram of measured horizontal betatron amplitudes together with a fit curve for emittance of 38.2 nm.

tudes probability for scattering parameters similar to those at IOTA: $p(A) = 2A_0^2 A/(A_0^2 + A^2)^2$. Two distributions are fit based on the tail of the amplitude distribution: empirical and exponential, with latter clearly showing poor agreement.

One can use the strong dependence of the vertical damping time on beam energy to estimate the energy of the electrons circulating in IOTA. Strongly suppressed transverse cou-

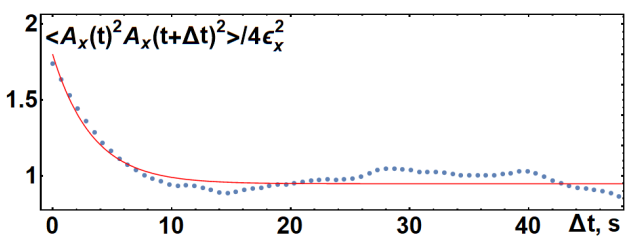

Figure 8: Autocorrelation of squared horizontal amplitudes vs. delay.

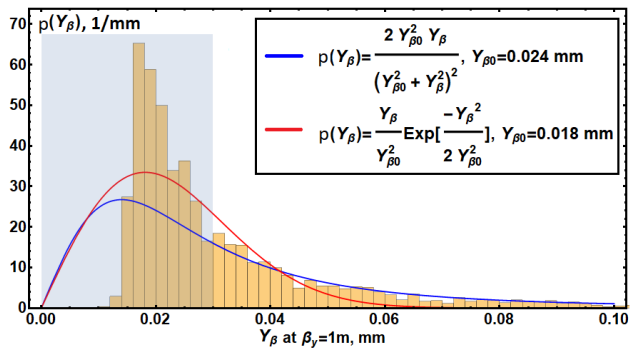

Figure 9: Measured distribution of vertical betatron amplitudes (yellow histogram) and fits for empirical (blie) and Gaussian beam (red) distributions. The shaded area was excluded from the fits because of the limited camera resolution (see text).

pling makes the vertical damping time almost independent of the lattice configuration. For a flat ring with revolution period T_0, the vertical damping rate is

$$\frac{1}{\tau_y} = \frac{1}{2}\frac{C_\gamma E^3}{2\pi T_0}\oint \frac{ds}{r^2}, \tag{5}$$

with $C_\gamma = (4\pi/3) r_e/(m_e c^2)^3 = 8.85\times10^{-5}$ m/GeV^3. The steep energy dependence gives favorable scaling for error propagation from damping time to energy. The resulting IOTA beam energy estimate is $E = 97.90 \pm 0.40(\text{stat}) \pm 0.35(\text{syst})$ MeV.

Residual Gas Characteristics and Machine Aperture

Information about residual gas pressure and composition can be extracted from beam lifetime and from the statistics of small-angle scattering events in the vertical plane. Both processes are dominated by Coulomb scattering on residual gas nuclei.

A cross section for single Coulomb scattering that deflects an electron in vertical plane by angle exceeding θ_{y0} can be calculated from the following formula:

$$\sigma(Z,\theta_{y0}) \simeq \frac{4\pi Z^2 r_e^2}{\gamma^2\beta^4\theta_{\text{screen}}^2}\left(1 - \frac{\theta_{y0}}{\sqrt{\theta_{y0}^2 + \theta_{\text{screen}}^2}}\right), \tag{6}$$

where $\theta_{\text{screen}} \simeq \alpha Z^{1/3}/(\beta\gamma)$.

The frequency of excitations to an amplitude exceeding A_y can be calculated by integrating mentioned cross section over

ISBN: 978-3-95450-214-1 ISSN: 2673-5490 doi:10.18429/JACoW-IPAC2021-THXB01

the ring circumference accounting for local beta function and effective gas pressure.

Figure 10 shows the dependence of normalized scattering frequencies (i.e., frequencies multiplied by $\theta^2_{y,\mathrm{eff}}$) on the effective vertical angle $\theta_{y,\mathrm{eff}} = A_y/\sqrt{\langle\beta_y\rangle}$, assuming constant partial pressures around the IOTA ring. Without screening effects, the normalized frequencies should be independent of scattering amplitude.

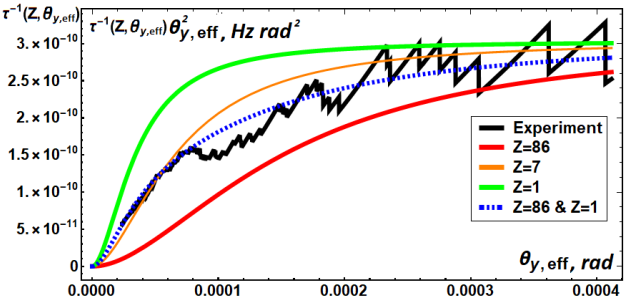

Figure 10: Dependence on the effective vertical angle $\theta_{y,\mathrm{eff}}$ of the scattering frequencies multiplied by $\theta^2_{y,\mathrm{eff}}$.

The plot show the experimental scattering frequencies together with 4 model curves for atomic numbers Z of 1 (hydrogen), 7 (nitrogen), 86 (radon) and for a combination of Z values 1 and 86. This combination, with partial coefficients $k_1 = 1$ and $k_{86} = 1.3(4) \times 10^{-4}$, showed the best fit, especially in the small-angle region, where most of the scattering events are concentrated. The resulting effective residual gas density is $n_{\mathrm{eff}} = 7.0(1.6) \times 10^8$ cm^{-3}.

The ring aperture can be estimated from the large-amplitude scattering cross section, together with the known beam lifetime and effective residual gas density. The available data does not allow to distinguish between restrictions in the vertical and the horizontal planes. The measured lifetime of 9100 s corresponds to apertures $A^2_{x,m} = A^2_{y,m} \simeq 12$ m, assuming equal maximum amplitudes in both planes.

RECONSTRUCTION OF AN ELECTRON TRAJECTORY IN A 6D PHASE SPACE

Using several PMTs to record times of arrivals of photons, synchronized with images from cameras, can be used to recover information about phase of all 3 modes and to improve precision of synchrotron amplitude measurements. This approach will work with linear lattices as cameras will be used to measure betatron amplitudes. In addition, long coherence of betatron oscillations is required, because PMTs can provide only very coarse and sparse detection of elcetron's position. For example, whether it is in the left, right, top or bottom halves of the phase space. With one detectable photon about every 100 turns data from coherent oscillations over about $10^5 - 10^6$ turns is necessary.

One of the best ways to measure electrons's position basing on a single photon detection is to use micro-channel plate (MCP) based detectors. They are commercially available, have single photon sensitivity with reasonable quantum efficiency of 10-20% and excellent time and spatial resolution. Having MCP based single photon detectors at all 8 optics diagnostics stages will enable a precise reconstruction of an electron's trajectory in the 6D phase space. This approach offers a promising method to study highly non-linear lattices through precise tracking of invariants of motion.

We plan to perform high-resolution measurements of 6D phase-space coordinates of a single electron in the IOTA storage ring over many revolutions. These true single-particle measurements will be further employed for benchmarking of long-term tracking simulations, for training of AI/ML algorithms, and ultimately for precise predictions of dynamics in current and future accelerators.

CONCLUSIONS

For the first time, to our knowledge, the dynamics of a single electron in a storage ring was tracked in all 3 dimensions using high-resolution synchrotron-light images acquired with digital cameras.

Data was taken at the Fermilab Integrable Optics Test Accelerator (IOTA) for both single electrons and for small countable numbers of electrons. A reliable and reproducible method to inject or remove a few electrons was developed. An absolute calibration of the camera intensity was implemented and its resolving power was evaluated. The beam lifetime at the lowest intensities was measured. In the central part of this work, we described how the horizontal, vertical and longitudinal oscillation amplitudes of a single electron were measured. From the time evolution of the oscillation amplitudes, several dynamical quantities were deduced, such as equilibrium emittances, momentum spread, damping times, and beam energy. The frequency distribution of residual-gas collisions events vs. scattering angle allowed us to estimate residual-gas pressure and composition and to give an approximate value for the machine aperture.

For the upcoming IOTA experimental runs, we plan to continue this research, adding to the camera images the synchronized acquisition of photon arrival times from the photomultipliers. This will allow us to record phase information for the betatron and synchrotron oscillations.

These measurements have a general scientific and pedagogic value, providing direct experimental insights into actual "single-particle dynamics" of an electron in a storage ring. In addition, these results provide information useful for machine commissioning, for beam instrumentation and diagnostics, and for verifying ring parameters obtained with more traditional techniques.

ACKNOWLEDGEMENTS

We would like to thank the entire FAST/IOTA team at Fermilab for making these experiments possible, in particular D. Broemmelsiek, K. Carlson, D. Crawford, N. Eddy, D. Edstrom, R. Espinoza, D. Franck, V. Lebedev, M. Obrycki, J. Ruan, and A. Warner.

REFERENCES

[1] C. Bernardini, "AdA: The first electron-positron collider", *Physics in Perspective*, vol. 6, pp. 156–183, 2004. doi:10.1007/s00016-003-0202-y

ISBN: 978-3-95450-214-1 ISSN: 2673-5490 doi:10.18429/JACoW-IPAC2021-THXB01

[2] L. Bonolis and G. Pancheri, "Bruno Touschek and AdA: from Frascati to Orsay", in memory of Bruno Touschek who passed away 40 years ago, on may 25th, 1978, Laboratori Nazionali di Frascati, Frascati, Italy, Rep. 18-05/LNF, May 2018.

[3] F. Riehle, S. Bernstorff, R. Fröhling, and F. P. Wolf, "Determination of electron currents below 1 nA in the storage ring BESSY by measurement of the synchrotron radiation of single electrons", *Nucl. Instrum. Methods Phys. Res. A*, vol. 268, pp. 262–269, 1988. doi:10.1016/0168-9002(88)90616-x

[4] G. Brandt *et al.*, "The Metrology Light Source—the new dedicated electron storage ring of PTB", *Nucl. Instrum. Methods Phys. Res. B*, vol. 258, pp. 445–452, 2007. doi:10.1016/j.nimb.2007.02.076

[5] R. Klein, R. Thornagel, and G. Ulm, "From single photons to milliwatt radiant power — electron storage rings as radiation sources with a high dynamic range", *Metrologia*, vol. 47, pp. R33–R40, Aug 2010. doi:10.1088/0026-1394/47/5/r02

[6] I. V. Pinayev *et al.*, "Experiments with undulator radiation of a single electron", *Nucl. Instrum. Methods Phys. Res. A*, vol. 341, pp. 17–20, 1994. doi:10.1016/0168-9002(94)90308-5

[7] A. N. Aleshaev *et al.*, "A study of the influence of synchrotron radiation quantum fluctuations on the synchrotron oscillations of a single electron using undulator radiation", *Nucl. Instrum. Methods Phys. Res. A*, vol. 359, pp. 80–84, 1995. doi:10.1016/0168-9002(96)88028-4

[8] I. V. Pinayev *et al.*, "A study of the influence of the stochastic process on the synchrotron oscillations of a single electron circulated in the VEPP-3 storage ring", *Nucl. Instrum. Methods Phys. Res. A*, vol. 375 , pp. 71– 73, 1996. doi:10.1016/0168-9002(95)01350-4

[9] C. Koschitzki *et al.*, "Highly sensitive beam size monitor for pA currents at the MLS electron storage ring", in *Proc. 1st Int. Particle Accelerator Conf. (IPAC'10)*, Kyoto, Japan, May 2010, paper MOPD084, pp. 894–896.

[10] A. Romanov, J. Santucci, G. Stancari, A. Valishev, and N. Kuklev, "Experimental 3- dimensional tracking of the dynamics of a single electron in the fermilab integrable optics test accelerator (IOTA)", Fermi National Accelerator Laboratory (FNAL), Batavia, IL, USA, Rep. FERMILAB-PUB-20-652-AD, Dec. 2020.

[11] S. Antipov *et al.*, "IOTA (Integrable Optics Test Accelerator): Facility and experimental beam physics program", *JINST*, vol. 12, pp. T03002–T03002, Mar. 2017. doi:10.1088/1748-0221/12/03/t03002

[12] A Romanov *et al.*, "Recent results and opportunities at the IOTA facility", Fermi National Accelerator Laboratory (FNAL), Batavia, IL, USA, Rep. FERMILAB-CONF-19-675-AD, 2020.

[13] V. Danilov and S. Nagaitsev, "Nonlinear accelerator lattices with one and two analytic invariants", *Phys. Rev. ST Accel. Beams*, vol. 13, p. 084002, Aug 2010. doi:10.1103/physrevstab.13.084002

[14] M. Church *et al.*, "Proposal for an accelerator R&D user facility at Fermilab's Advanced Superconducting Test Accelerator (ASTA)", Fermi National Accelerator Laboratory (FNAL), Batavia, IL, USA, Rep. FERMILAB-TM-2568, Fermilab, Oct. 2013.

[15] A. L. Romanov *et al.*, "Commissioning and Operation of FAST Electron Linac at Fermilab", in *Proc. 9th Int. Particle Accelerator Conf. (IPAC'18)*, Vancouver, Canada, Apr.-May 2018, pp. 4096–4099. doi:10.18429/JACoW-IPAC2018-THPMF024

[16] A. L. Romanov, G. T. Kafka, S. Nagaitsev, and A. Valishev, "Lattice Correction Modeling for Fermilab IOTA Ring", in *Proc. 5th Int. Particle Accelerator Conf. (IPAC'14)*, Dresden, Germany, Jun. 2014, pp. 1165–1167. doi:10.18429/JACoW-IPAC2014-TUPRO058

[17] A. Valishev, N. Kuklev, A. Romanov, G. Stancari, and S. Szustkowski, "Nonlinear integrable optics (NIO) in IOTA Run 2", Fermi National Accelerator Laboratory (FNAL), Batavia, IL, USA, Rep. Beams-doc-8871, Nov. 2020.

[18] S. A. Antipov, S. Nagaitsev, and A. Valishev, "Single-particle dynamics in a nonlinear accelerator lattice: Attaining a large tune spread with octupoles in IOTA", *JINST*, vol. 12, pp. P04008– P04008, Apr. 2017. doi:10.1088/1748-0221/12/04/p04008

[19] N. Kuklev, Y. K. Kim, S. Nagaitsev, A. L. Romanov, and A. Valishev, "Experimental Demonstration of the Henon-Heiles Quasi-Integrable System at IOTA", in *Proc. 10th Int. Particle Accelerator Conf. (IPAC'19)*, Melbourne, Australia, May 2019, pp. 386–389. doi:10.18429/JACoW-IPAC2019-MOPGW113

[20] G. Stancari *et al.*, "Notes on the design of experiments and beam diagnostics with synchrotron light detected by a gated photomultiplier for the Fermilab superconducting electron linac and for the Integrable Optics Test Accelerator (IOTA)", Fermi National Accelerator Laboratory (FNAL), Batavia, IL, USA, Rep. FERMILAB-FN-1043-AD-APC, 2017.

[21] I. Lobach *et al.*, "Observation of Undulator Radiation Generated by a Single Electron Circulating in a Storage Ring and Possible Applications", presented at the 12th Int. Particle Accelerator Conf. (IPAC'21), Campinas, Brazil, May 2021, paper WEPAB087, this conference.

[22] J. Safranek, "Experimental determination of storage ring optics using orbit response measurements", *Nucl. Instrum. Meth. A*, vol. 388, pp. 27–36, 1997. doi:10.1016/s0168-9002(97)00309-4

[23] V. Sajaev, V. Lebedev, V. Nagaslaev, and A. Valishev, "Fully Coupled Analysis of Orbit Response Matrices at the FNAL Tevatron", in *Proc. 21st Particle Accelerator Conf. (PAC'05)*, Knoxville, TN, USA, May 2005, paper MPPE065, pp. 3662–3664.

[24] A. Romanov *et al.*, "Correction of magnetic optics and beam trajectory using LOCO based algorithm with expanded experimental data sets", Fermi National Accelerator Laboratory (FNAL), Batavia, IL, USA, Rep. FERMILAB-PUB-17-084-AD-APC, Mar. 2017.

[25] G. Stancari, "Beam lifetime from time intervals between single-electron losses in storage rings", Fermi National Accelerator Laboratory (FNAL), Batavia, IL, USA Rep. FERMILAB-FN-1116-AD, Fermilab, to be published.